IOP Conf. Series: Materials Science and Engineering **655** (2019) 012002 doi:10.1088/1757-899X/655/1/012002

Effect of the quench temperature on the mechanical properties of a medium C Mn high Si steel during Q&P heat treatment process

V Kurup*, C W Siyasiya and R J Mostert

Department of Metallurgy and Material Science, University of Pretoria, South Africa

E-mail: vinod.kurup@up.ac.za

Abstract. A steel of composition Fe-0.2C-3Mn-2Si-0.5Al was fully austenized followed by a quench and partitioning heat treatment process (Q&P). The quench temperature was varied, which resulted in different volume fractions of retained austenite (RA) and martensite. Analysis of the phase evolution and the resulting microstructures during the Q&P process were carried out using different techniques namely, - dilatometry, FEG SEM, EBSD, and neutron diffraction. Mechanical properties were evaluated by standard tensile tests on samples quenched to different temperatures. The partitioning process was evaluated by dilatometry. The volume fraction of the RA was determined by neutron diffraction. It was found that the volume fraction of RA increased with an increase in the quench temperature contrary to the Speer model. It was also observed that the presence of bainite, which formed during the quench and partitioning temperature significantly stabilized the RA by carbon partitioning. The tensile test results indicated the optimum quench temperature for the best combination of strength and ductility and contrary to expectation, this did not occur in the specimen with the maximum amount of RA. In other words, the mechanical properties of the steel undergoing a Q&P process is influenced by the quench temperatures and is also affected the phase evolution which occurs during both the quench and partitioning process.

1. Introduction

The average use of advanced high strength steel (AHSS) has increased significantly over the past decade in the automobile sector [1]. This was mainly due to the change in material concepts to meet the requirements of OEMs in terms of performance and safety consideration. Third generation AHSS is based on multiphase microstructure targeting strength higher than 1000 MPa [2]. Speer et al. [3] proposed a quench and partitioning (Q&P) process as one of the methods to manufacture third generation AHSS. This process consists of heating steel above Ac_3 to obtain a fully austenitic structure, or between Ac_1 and Ac_3 to obtain partial austenitic structure. It is then quenched to a predetermined temperature between the M_s and M_f to obtain a certain fraction of martensite and retained austenite (RA). It is then reheated to a temperature well below Ac_1 for a certain time interval which enables the transfer of carbon from martensite to austenite, this being referred to as the partitioning stage. Finally, the sample is quenched back to room temperature. In this manner, a multiphase microstructure consisting of tempered martensite, austenite, fresh martensite and ferrite, in the case of partial austenitisation, is obtained. Some authors [4,5] have reported competing reactions, such as carbide precipitation and austenite decomposition to bainite during the partitioning stage.

In the present work, the evolution of microstructures at various quench temperatures during the Q& P process was studied. Using Speer's CCE (constraint carbon equilibrium) model [3] the optimum quench temperature at which maximum RA was obtained. The different quench temperatures were selected above and below the optimum quench temperature and the RA was measured using neutron diffraction. Dilatometry was used to identify the austenite decomposition at the partitioning temperature. Tensile testing was performed to evaluate to see the effect of microstructure on mechanical properties. The present study showed that the formation of bainite did influence the amount of retained austenite present in the microstructure. At quench temperatures greater than the optimum quench temperature the amount of RA was more than predicted by the Speer model [3]. The optimum quench temperature sample, however, exhibited better ductility than the sample with a larger amount of retained austenite.

2. Experimental Procedure

2.1 Material

A high Si content steel was produced in the lab with a composition of Fe-0.27%C -2.8%Mn -2.2% Si-0.75% Cr and 0.5% Al using induction melting. The cast ingot was hot rolled and forged to a round bar of diameter 13mm and length 30cm. Silicon was specifically added to prevent cementite formation [6]. Even though Si is a ferrite stabilizer, it also stabilizes the RA by retardation of cementite formation.

2.2 Dilatometer Experiments

A series of dilatometer experiments were conducted to obtain critical transformation temperatures before the start of the Q&P heat treatment process. Cylindrical samples 10mm x 5mm diameter were used to carry out the heat treatment in the B*ä*hr 805 D^{TM} dilatometer. The specimen was placed between two quartz rods, heated by an induction coil and cooled using He gas. Both the temperature and change in length as a function of time were recorded. Using the Speer model [3], the optimum quench temperature was calculated, which gives the temperature at which the maximum RA fraction can be obtained. The optimum quench temperature was calculated as 225^{o}C. Specimens were quenched at different temperatures above and below the predicted optimum quench temperature. The partitioning process was carried out at 400 ^{o}C before quenching to room temperature. The quench temperatures were 180, 200, 220, 225, 240 and 260 ^{o}C. The heat treatment cycle followed is show in Figure 1. Using the lever rule, the fraction of RA and martensite at each quench temperature was deduced from the change in length vs temperature plot obtained from the dilatometry.

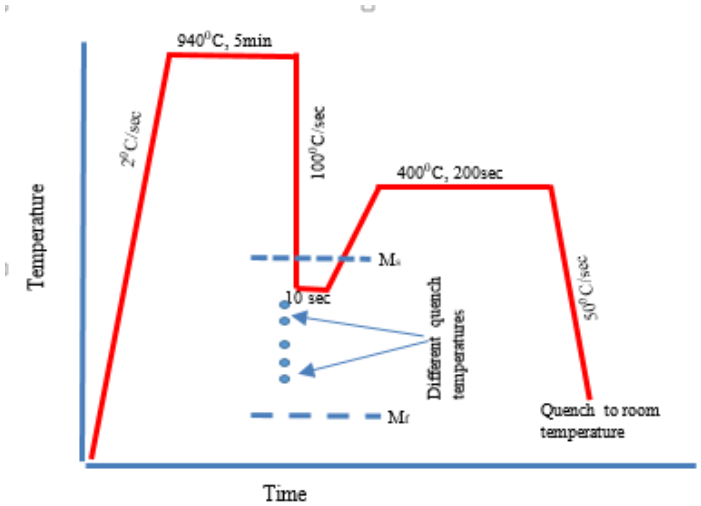

Figure 1. Schematic diagram of quench and partitioning heat treatment with different quench temperatures.

2.3 Neutron Diffraction

The volume fraction of phases after the Q&P heat treatment was determined by neutron diffraction performed at Necsa (Nuclear Energy Council of South Africa). The advantage of neutron diffraction in

comparison to XRD is that the neutron beam penetrate deeper into the sample. The intensity and positions of each peak were analysed using "TOPAZ 4.2" peak fitting software. Rietveld analysis [7] was used for quantification of the volume fraction of phases. The lattice parameters of austenite and martensite were obtained from the diffraction data. In the present study, the C content of the RA was determined using the empirical relationship between lattice parameter and composition [8] as shown in equation (1):

$$a\,(\gamma) = 0.3556 + 0.00453w_c + 0.00095w_{mn} + 0.00056w_{al} + 0.0006w_{c\,r} - 0.0002w_{ni} \qquad \text{eq (1)}$$

where a (γ) is the lattice parameter of austenite in nm w (%) = weight % of elements.

2.4 Microstructural analysis

The standard sample preparation for metallographic analysis was followed. The microstructures were examined after each Q&P heat treatment cycle by a JEOL FEG-SEM at an accelerating voltage of 5kV. From heat treated samples 3mm diameter disc were cut out and metallographically ground to a thickness of less than 50 µm. These samples were subjected to twin-jet polishing in a "Tenopol 5" jet polishing machine. The jet polishing was carried out using 5% perchloric acid and 95% glacial acetic acid at approximately -15°C. Transmission Kikuchi Diffraction (TKD) was carried out on jet polished specimens The TDK analysis was performed at an accelerating voltage of 30 kV, tilt angle of 20° and a step size of 50 nm. The data was analysed using Aztech from Oxford Instruments.

2.5 Tensile testing:

K-Type thermocouples were spot welded to the test specimens to ensure correct temperature was attained during the heat treatment carried out in a salt bath. Sub size specimens with round cross-section of 6mm diameter and 30 mm gauge length were machined according to ASTME8/E8M-09 [9]. The tensile testing was carried out using MTS Criterion® series 45 tensile machine, on selected specimens quenched to 180, 225 and 260°C.

3. Results

3.1 Thermodynamic analysis

Thermo-Calc and JMatpro thermodynamic softwares were used to calculate the phase fractions and continuous cooling transformation (CCT) diagram of the experimental steel, see figure 2

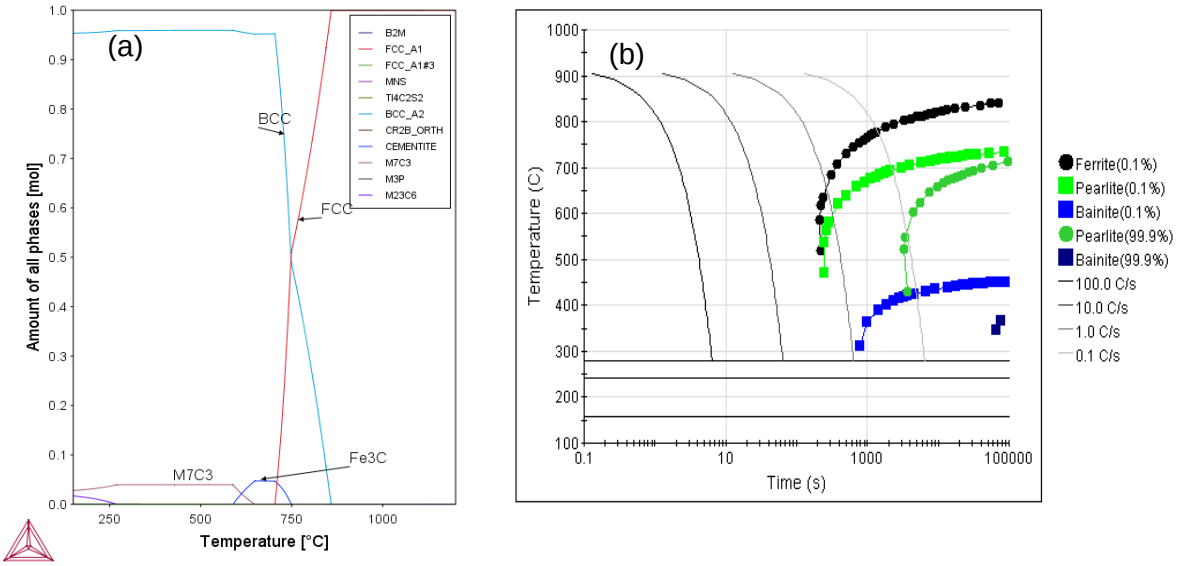

Figure 2. (a) Calculated phase fractions for a range of temperatures using Thermo-Calc (b) CCT diagram of experimental steel using JMatpro

Figure 2(a) shows the phase fraction at various temperatures. It also shows the presence of carbides at low temperature and cementite being stable above 550°C. The presence of Si in the steel shifts the formation of cementite to a higher temperature. Transition carbide stability is not affected by the presence of silicon, and its presence is shown in the temperature range of 200-250°C. Partitioning process in the Q&P heat treatment was carried out at 400°C, and from Figure 2(b), the CCT diagram predicts the formation of bainite at this temperature.

3.2 Optimum temperature calculation by constraint carbon equilibrium (CCE) model

Speer model [3] was used to estimate the optimum quench temperature which produced the maximum RA. The amount of martensite present at each temperature was determined by the K-M equation (2)

$$V_{primary}^{\alpha} = 1 - \exp(-\alpha(M_s - T)) \qquad \text{eq (2)}$$

where $V_{primary}^{\alpha}$ is the fraction of primary martensite formed at the first quench
ά = rate parameter assumed 0.011
M_s= Martensite start temperature.

M_s temperature is based on the empirical equation(3) [11]

$$M_s = 545\text{-}330*\%C+2*\%Al+7*\%Co-14*\%Cr-13\%Cu-23\%Mn-5\%Mo -4\%Nb-13\%Ni-7\%Si+3\%Ti+4\%V \qquad \text{eq (3)}$$

Using Equation 3, the M_s calculated was 366°C and this was close to the value determined by the dilatometer. During the partitioning stage, carbon is assumed to fully partition to austenite and the carbide precipitation is avoided. As a result, the carbon- enriched austenite has a lower M_s which then leads to stabilization of austenite at room temperature. If the carbon partitioning is not sufficient during the partitioning stage, the austenite after the second quench would transform to secondary martensite .The carbon content of the carbon enriched austenite was determined by CCE condition.[3] which is then substituted back in the M_s Equation 3 to obtain the new M_s for the carbon-enriched austenite. K-M equation 2 is then reapplied with new M_s to get the fraction of secondary martensite ($V_{secondary}^{\alpha}$). The optimum quench temperature was obtained when the M_s was equal to room temperature i.e 25°C. Figure. 3 shows the optimum quench temperature was 225°C with maximum retained austenite of 21.5%.
The final austenite content (V_{γ}^{final}) was obtained using equation 4.

$$V_{\gamma}^{final} = 1 - V_{primary}^{\alpha} - V_{secondary}^{\alpha} \qquad \text{eq (4)}$$

where $V_{secondary}^{\alpha}$ = secondary martensite formed after second quench

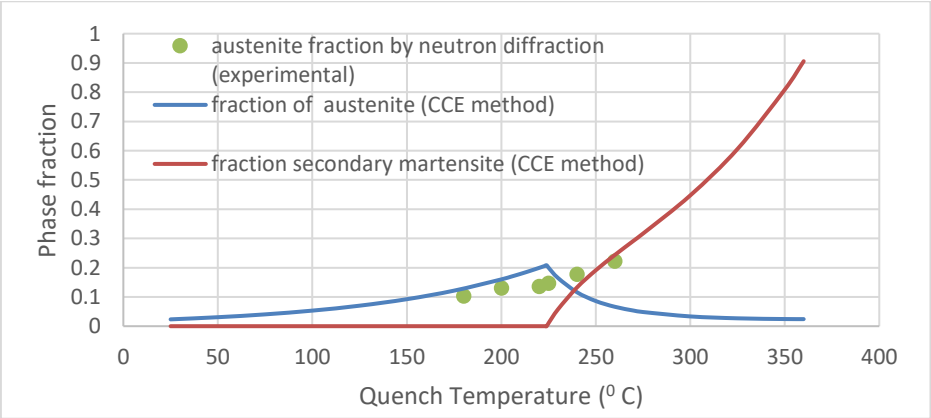

Figure 3. Volume fraction of phases (austenite and secondary martensite) at different quench temperature obtained by the CCE method and fraction of austenite determined experimentally by neutron diffraction

3.3 Dilatometry

The critical temperatures A_{c1}, A_{c3}, and M_s were determined from dilatometer experiments and were found to be 750, 860 and 370ºC respectively. Figure 4 shows Q&P process carried out at different quench temperatures in dilatometer. During cooling, the first expansion took place due to martensitic transformation and then at the partitioning stage there were various degrees of expansion as indicated by a red circle in the 240 and 260ºC quench case. During the second quench, there was further expansion indicating the formation of secondary martensite as seen in Figure. 4 (deviation indicated by a blue line in the case 260ºC quench). The portion of the isothermal dilation during partitioning was enlarged and plotted separately in Figure 5. The 220ºC quench, exhibited an initial expansion which was followed by a contraction, while the 260ºC quench exhibited the highest expansion as seen in Figure 5. From Figure 5 for 200ºC and 220ºC quench, there was initial expansion which was related to bainite formation and followed by a contraction which was attributed to the tempering of martensite.

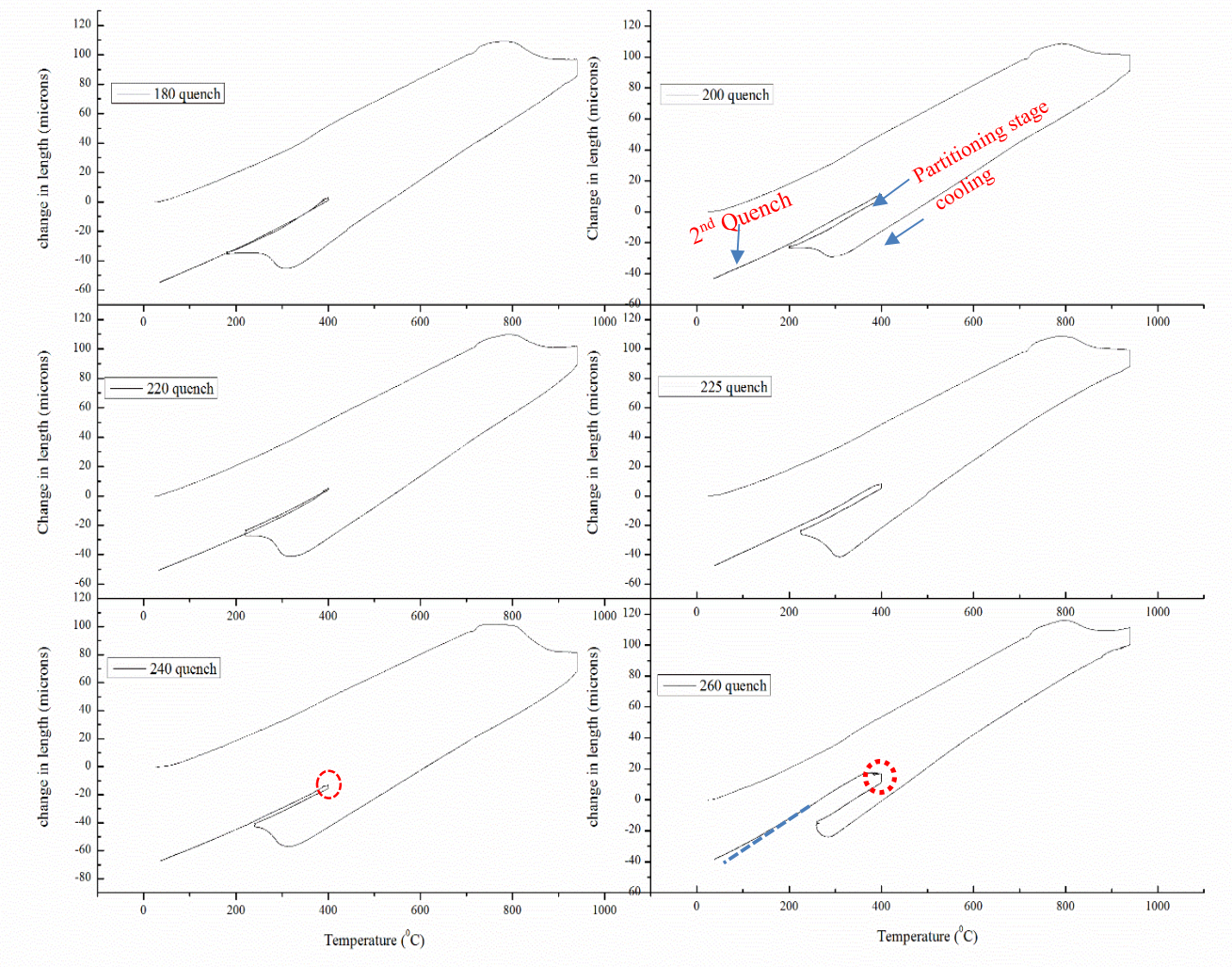

Figure 4. Change in length with the temperature at various quench temperatures during the Q&P heat treatment

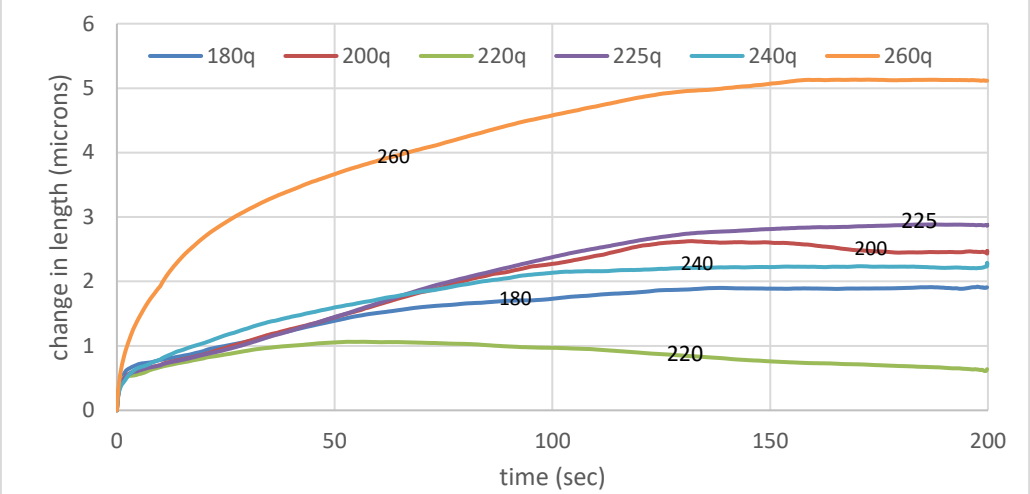

Figure 5. Change in length with time during the isothermal partitioning stage at 400ºC

3.4 Neutron diffraction

The neutron diffraction results for the various quench temperatures are presented in Figure 6a. The (111) peak intensity of RA increased with increase in the quench temperatures. The volume fraction of RA obtained from the Rietveld analysis is shown in Figure 3. The results in Figure 3 indicate that the volume fraction of RA was lower than the value predicted by the Speer model up to 225ºC and beyond 225ºC it was higher than the predicted values. The reason for this difference can be attributed to the formation of bainite during the partitioning stage.

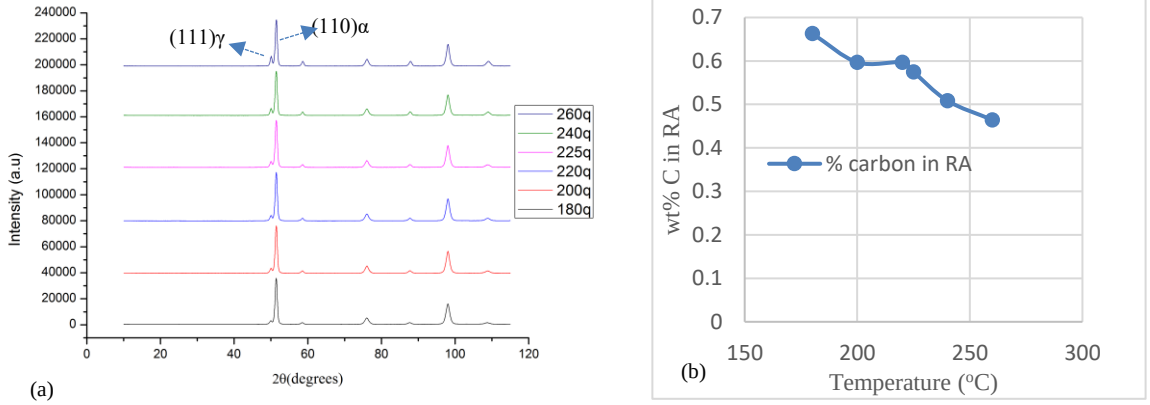

Figure 6. (a) Neutron diffraction of samples quenched at different temperatures during the Q&P heat treatment and (b) weight % C in RA at various quench temperatures

Figure 6(b) shows the weight %C in the RA after the Q&P treatment at various quench temperatures. This was determined by equation 1 using the lattice parameter obtained from the neutron diffraction results. As expected, the amount of C in the RA decreased with an increase in the quench temperature due to an increase in the amount of RA. The maximum carbon content was found to be 0.66 wt. % at 180ºC quench temperature.

3.5 Microstructure analysis

The microstructures of the samples quenched at various temperatures are presented in Figure 7. In the sample quenched to room temperature, Figure 7a, the microstructure consisted of needles of martensite of different orientations with no carbides present. In Figure 7 b, c, and d, the microstructure was multiphase and complex. It consisted of following features (a) Martensite (M),elongated lath-shaped without carbides,(b) Bainite which was present in two different forms (B1)thick irregular with wavy edges also without carbides and (B2)small acicular units aligned parallel to each other.(c) Tempered martensite (TM), laths with sharp tip with carbide [12]. The RA was present in the form of thin films which was difficult to detect by SEM. However the TKD analysis of the sample quenched at 260 ^{o}C, shows the presence of RA and epsilon carbide as seen in Figure 8.

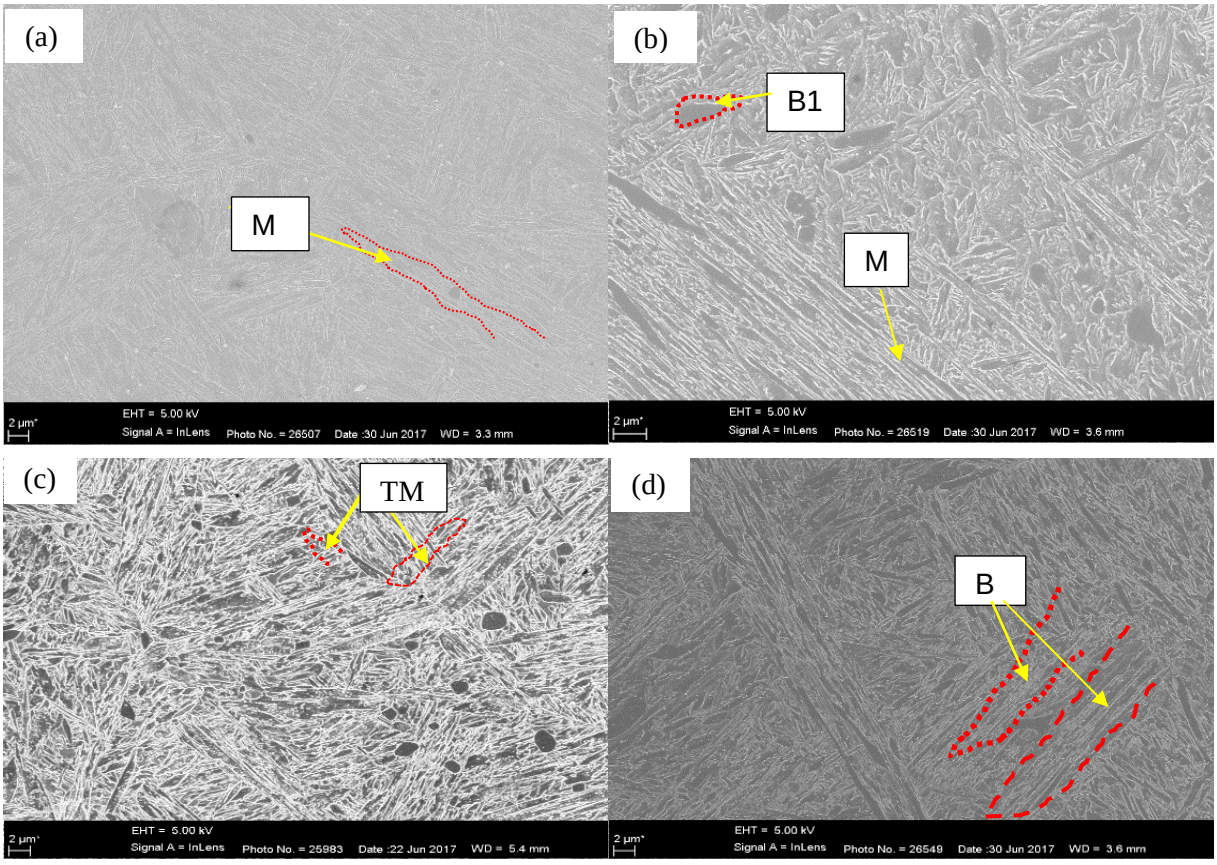

Figure 7. SEM micrographs taken in SE mode (a) direct quench to room temperature (b) 180^{o}C quench (c) 240^{o}C quench and (d) 260^{o}C quench

Figures 8(a) and (b) show the band contrast image and phase colour map from TKD analysis of 260^{o}C quench sample. Figure 8b,showed the distribution of thin films of RA occurred between the martensite laths and bainitic ferrite acicular structure in agreement with Navarro et al [12]. It also revealed the presence of epsilon carbide in the martensite lath structure. There were regions not identified by TKD analysis as shown by the dark contrast. These regions corresponded to either secondary martensite or untempered martensite formed during the second quench [13]. Marito et al. [14] reported that the high dislocation density is known to lower the quality of Kikuchi bands in EBSD patterns and deteriorates the phase identification. The presence of Si prevented the formation of Fe_3C phase but did not prevent the epsilon carbide formation [15].

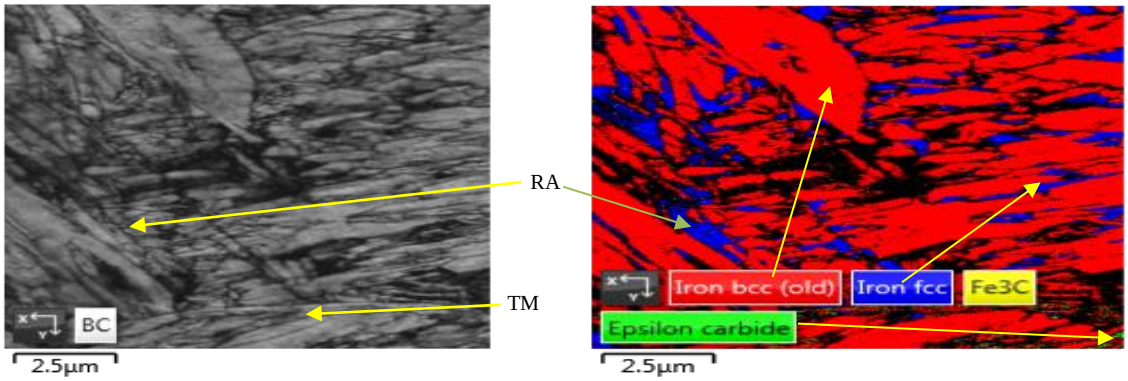

Figure 8. TKD micrograps showung (a) Band contrast and (b) Phase colour map of sample quenched at 260ºC

3.6 Mechanical properties:

The tensile test results for samples subjected to Q&P heat treatment at three different quench temperature are summarised in table 1

Table 1. Tensile test results

Quench Temperature(^{0}C)	Tensile strength (MPa)	Yield Strength (MPa)	% Elongation
180 (low)	1360± 15	1070±10	13.5±0.6
225 (optimal)	1320± 10	975±10	15.3±0.6
260 (high)	1440±20	670±10	13.3±0.8

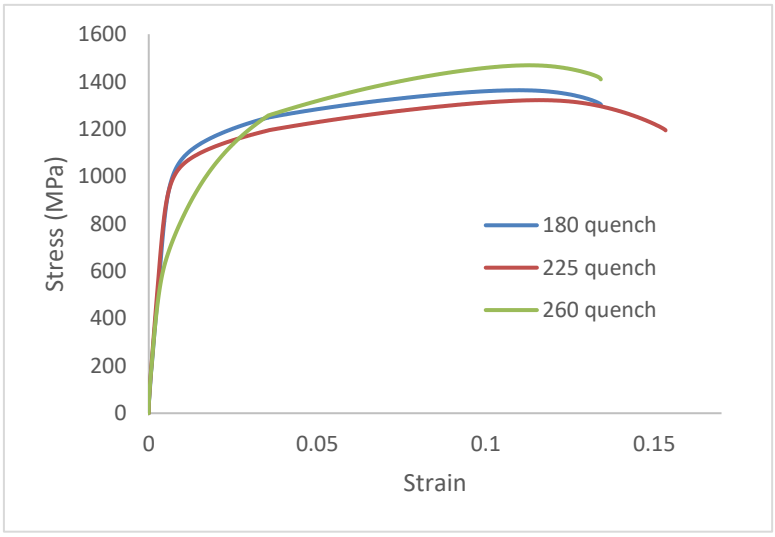

Figure 9. Stress vs strain plot for a samples subject to Q&P process at three different quench temperature

The sample quenched at low temperature (180ºC quench) exhibited the highest yield strength of 1070±10. At 225ºC quench, both the yield and tensile strength decreased slightly but the average total elongation slightly improved to 15.3%. At high quench temperature of 260ºC, the sample had low yield to tensile ratio .This property is attractive for crash worthiness applications requiring high levels of energy absorption and work hardening.

4. Discussion

The Speer model [3] predicted the optimum quench temperature of 225ºC where 21% RA would be obtained. However the neutron diffraction results showed maximum RA at 260ºC. This difference was

associated with the formation of bainite during isothermal partitioning process at 400ºC. Figure 5 shows the expansion taking place during the partitioning process at various quench temperatures. The length change due to C partitioning has been found to be around 0.03% [16] which is quite small in comparison to what is seen in Figure 5. This larger length change was due to the isothermal decomposition of austenite to bainite along with carbon partitioning [17] . For the low-temperature quench at 200ºC and 220ºC, the initial expansion was due to bainite formation and was then followed by contraction due to the tempering of martensite. In the case of the low quench temperatures, the C content in the austenite was high i.e. it exceeds the T_0 value (T_0 is the temperature where free energy of parent and product phase is equal) [15]. The C enrichment in austenite during partitioning was due to bainite formation which ejects carbon to the surrounding austenite. Therefore, RA was stabilized and no further bainite transformation took place as the C in austenite exceeded the C limit at T_0 . This incomplete austenite to bainite transformation can be related to the initial expansion which is seen in the case of 200ºC and 220ºC quenches. In the 260ºC quench, the C concentration in the austenite was low as calculated from lattice parameter values due to high volume fraction of RA. Since carbon content was below the T_0 value this lead to transformation of austenite to bainite and the rejection of carbon from bainite lead to stabilization of austenite. This led to higher RA stabilized at 260ºC quench than what was calculated based on CCE [3] .

The behaviour of the stress-strain curve is a function of dislocation density evolution and this is governed by the microstructure [13]. After the Q& P process, the microstructure consisted of tempered martensite, RA and also secondary martensite for the high-temperature quench. In addition, the RA underwent strain-induced martensitic transformation (SIMT). In the 180ºC quench, the stability of the RA was higher due to the higher C content (Figure 6 b), so, the extent of the RA to SIMT was expected to be low. This resulted in the higher yield strength. On the contrary, the 260ºC quench had higher fraction of RA but due to its low C content in RA, its stability was low. Therefore the extent of RA to SIMT was greater leading to low yield strength to tensile strength ratio ($R_p./R_m$) and high work hardening observed.

The presence of secondary martensite (Figure. 4) for the 260ºC quench sample led to relatively low ductility. It has been reported elsewhere that untempered martensite exhibits a low yield strength and smooth elastic-plastic transition [13] . There are several possibilities for the 260ºC quench flow behaviour as proposed by different authors viz. 1) Takaki et al [18] suggested that high density of fresh dislocation are created during the phase transformation and these dislocations have high mobility eliminating yield point effects and causing a rounded stress-strain curve at lower loads; 2) Allain et al [19] suggested that inhomogeneous C distribution in as-quenched martensite can result in a austenite martensite phase mixture containing different hardness. These regions may yield at different stress on loading. In the case of the optimum quench (225ºC), there is no secondary martensite formation.and lower fraction of RA compared to high temperature quench (260ºC) The high C in RA lead to higher yield strength and no secondary martensite formation gave higher ductility in the optimum quench sample

5. Conclusions

The Q&P process of the medium C Mn high Si steel was studied using different techniques and the following observations were made:

- The sample quenched at 260^0C yielded the highest amount RA after the Q&P process. This was attributed to the bainite formation which enriched the austenite to stabilize it.
- The discrepancy between predicted and actual amount of RA was attributed the bainite formation during Q&P process which was not considered in the prediction of the optimum quench temperature which yields maximum RA based on Speer model.
- The optimum quench (225ºC) exhibited the best combination of strength and ductility, in spite of lower RA. This was due to the absence of secondary martensite and a higher stability of retained austenite.

6. Acknowledgments:
The authors would like to acknowledge Ferrous Metal Development Network (FMDN) for the financial support. The authors also want to acknowledge NMMU (Nelson Mandela Metropolitan University) for the assistance in TKD analysis. NECSA and Prof JPR de Villiers of University of Pretoria for the assistance in neutron diffraction and rietveld analysis.

7. References

1. Lesch C, Kwiaton N, Klose FB. Advanced High Strength Steels (AHSS) for Automotive Applications − Tailored Properties by Smart Microstructural Adjustments. Vol. 88, Steel Research International. Wiley-VCH Verlag; 2017.
2. Kuziak R, Kawalla R, Waengler S. Advanced high strength steels for automotive industry. Arch Civ Mech Eng [Internet]. 2008;8(2):103–17. Available from: http://www.sciencedirect.com/science/article/pii/S1644966512601976
3. Speer J, Matlock DK, De Cooman BC, Schroth JG. Carbon partitioning into austenite after martensite transformation. Acta Mater. 2003;51(9):2611–22.
4. De Moor E, Speer JG. Bainitic and quenching and partitioning steels. In: Automotive Steels: Design, Metallurgy, Processing and Applications. Elsevier Inc.; 2016. p. 289–316.
5. Toji Y, Miyamoto G, Raabe D. Carbon partitioning during quenching and partitioning heat treatment accompanied by carbide precipitation. Acta Mater. 2015;86:137–47.
6. Zhu L Juan, Wu D, Zhao X Ming. Effect of Silicon Content on Thermodynamics of Austenite Decomposition in C-Si-Mn TRIP Steels. J Iron Steel Res Int. 2006;13(3):57–61.
7. David WIF. Powder diffraction: Least-squares and beyond. J Res Natl Inst Stand Technol [Internet]. 2004;109(1):107. Available from: https://nvlpubs.nist.gov/nistpubs/jres/109/1/j91dav.pdf
8. Van Dijk NH, Butt AM, Zhao L, Sietsma J, Offerman SE, Wright JP, et al. Thermal stability of retained austenite in TRIP steels studied by synchrotron X-ray diffraction during cooling. . Acta Materialia 53 (2005) 5439–5447
9. ASTM E8/8M [Internet]. ASTM. 2016. Available from: www.astm.org
10. Koistinen D.P and Marburger R.E. A general equation presecribing the extent of austenite - martensite transformation in pure iron carbon alloys and plain carbon steels. Acta Metall Mater. 1959;7:59–60.
11. Hsu T. An approximate approach for the calculation of Ms in Fe-base alloys. J Mater Sci 1985;20:23–31.
12. Navarro-López A, Hidalgo J, Sietsma J, Santofimia MJ. Characterization of bainitic/martensitic structures formed in isothermal treatments below the Ms temperature. Mater Charact. 2017;128(March):248–56.
13. Seo EJ, Cho L, Estrin Y, De Cooman BC. Microstructure-mechanical properties relationships for quenching and partitioning (Q&P) processed steel. Acta Mater. 2016;113.
14. Morito S, Nishikawa J, Maki T. Dislocation Density within Lath Martensite in Fe-C and Fe-Ni Alloys. ISIJ Int. 2003;43(9):1475–7.
15. Ravi AM, Sietsma J, Santofimia MJ. Exploring bainite formation kinetics distinguishing grain-boundary and autocatalytic nucleation in high and low-Si steels. Acta Mater. 2016;105:155–64.
16. Santofimia MJ, Zhao L, Sietsma J. Volume Change Associated to Carbon Partitioning from Martensite to Austenite [Internet]. Vols. 706–709, Materials Science Forum. 2012. p. 2290–5. Available from: http://www.scientific.net/MSF.706-709.2290
17. Hajyakbary F, Sietsma J, Miyamoto G, Furuhara T, Santofimia M. Interaction of carbon partitioning, carbide precipitation and bainite formation during the Q&P process in a low C steel. Acta Mater. 2016 Feb 1;104:72–83.
18. Takaki S, Fujimura Y, Nakashima K, Tsuchiyama T. Effect of Dislocation Distribution on the Yielding of Highly Dislocated Iron. Mater Sci Forum [Internet]. 2007;539–543:228–33. Available from: https://www.scientific.net/MSF.539-543.228

19. Allain S, Bouaziz O, Takahashi M. Toward a New Interpretation of the Mechanical Behaviour of As-quenched Low Alloyed Martensitic Steels. ISIJ Int. 2012;52(4):717–22.